MSUCP—25

MICHIGAN STATE UNIVERSITY

CYCLOTRON PROJECT

The Nonlinear Coupling Resonance Exhibited by an Elastic Pendulum*

M. M. Gordon

Department of Physics — Cyclotron Laboratory

East Lansing, Michigan

December 1970

*This work was partially supported by the National Science Foundation

The Nonlinear Coupling Resonance Exhibited by an Elastic Pendulum*

M. M. Gordon
Physics Department-Cyclotron Laboratory
Michigan State University
East Lansing, Michigan 48823 USA

ABSTRACT

The simple elastic pendulum provides a vivid demonstration of nonlinear coupling resonance phenomena when the frequency of its vertical (spring) oscillations is just twice that of its horizontal (pendulum) oscillations. These nonlinear phenomena are analyzed using standard perturbation theory. The observed transfer of energy between the normal modes of the system is fully explained by the theory, whose accuracy is confirmed by computer calculations. The stable periodic modes, which correspond to unique parabolic trajectories, are also investigated using both analytical and computer techniques. These results are then compared with experimental data.

*This work was partially supported by the National Science Foundation.

CONTENTS

Section		Page
I.	Introduction	1
II.	Description of Transfer Cycle	7
III.	Equations of Motion	12
IV.	Nonlinear Resonance Condition	15
V.	Perturbation Theory	18
	A. Modified Lissajous Figures	23
VI.	Invariant Curves	25
	A. Phase Space Plots	29
VII.	Transfer Cycle Periods	31
VIII.	Stable Periodic Modes	35
	A. Computer Results	38
	B. Experimental Data	40
IX.	Concluding Remarks	43
References		46
Figures 1 - 7		47ff

I. INTRODUCTION

Nonlinear resonances comprise a group of very interesting phenomena, and the study of these resonances should certainly be included in any up-to-date course on mechanics. The theory of these resonances forms a part of "nonlinear mechanics" which was developed during the first half of this century in order to treat certain problems in celestial mechanics and in electrical circuits containing nonlinear elements.[1] More recently, this theory has found important applications in the orbit dynamics of alternating gradient synchrotrons and isochronous cyclotrons, where the presence of nonlinear resonances strongly influences the choice of machine parameters.[2] Consequently, this subject has practical importance as well as intrinsic interest.

The most widely known examples of nonlinear resonances involve a harmonic oscillator driven by a nonlinear periodic force. Nonlinear resonances can, however, occur in strictly conservative systems having at least two degrees of freedom. These cases correspond to "nonlinear coupling resonances" which manifest themselves through a significant transfer of energy back and forth between the normal modes of the system. The simplest nonlinear coupling resonance occurs in a system having only two normal modes (x and y) which satisfy the frequency relation: $\omega_x = 2\omega_y$, and also

having a residual potential energy which contains an xy^2 term. The elastic pendulum provides an excellent example of such a system.[3] As a device for demonstrating a nonlinear resonance, the elastic pendulum has the following desirable features: it is purely mechanical, it requires no driving force, it can be constructed very easily, and it displays a strong coupling action which is both readily apparent and rather baffling to the uninitiated observer. This deceptively simple device therefore furnishes an appropriate means for introducing the student to the subject of nonlinear resonances.

The elastic pendulum, which is shown in Fig. 1, consists of a steel spring with a massive bob attached to its lower end, and with its upper end connected by a thin cord to a rigid support. The angular frequencies of its vertical (spring) oscillations and its horizontal (pendulum) oscillations are respectively given by:

$$\omega_x = (k/m)^{1/2}, \quad \omega_y = (g'/L)^{1/2}, \tag{1}$$

where k is the force constant of the spring, m is the effective mass of the bob, L is the distance from the point of support to the center of the bob, and g' is a modified gravity constant. If m_b and m_s are the masses of the bob and the spring, then the following definitions and relations prevail:

$$m = m_b + m_s/3, \tag{1a}$$

$$mg' = (m_b + \tfrac{1}{2}m_s)g, \tag{1b}$$

$$k(L - L_o) = mg', \tag{1c}$$

where L_o is the extrapolated pendulum length in the limit of zero gravity. Given a suitable spring, the values of k, m_s, and L_o can all be measured. The particular value of m_b required to fulfill the frequency condition: $\omega_x = 2\omega_y$, can then be calculated from the formula:

$$kL_o = 3(m_b + \tfrac{1}{2}m_s)g, \tag{2}$$

which is derived from the relations above. The length of the supporting cord should be made quite variable. This cord length, which affects ω_y but not ω_x, can be used to tune the system after the bob has been mounted. The coupling action will become very apparent when the system is close to resonance, and it will be observed that the tuning of this resonance is not critical.

The particular model of the resonant elastic pendulum shown in Fig. 1 is the one used for our demonstrations and experiments. This model has the following measured parameters: $k \approx 7090$ dyne/cm, $m_b \approx 92$ gm, $m_s \approx 5$ gm, $L \approx 52.3$ cm at resonance. Using these values in Eq. (1), the vertical and horizontal oscillation periods are found to be: $\tau_x = 0.723$ sec and $\tau_y = 1.45$ sec, respectively. The value for τ_x was confirmed by an independent measurement of this period.

To demonstrate the resonance coupling action, the bob is displaced vertically downward by about one inch (5% of L) and then released from rest. The bob will initially perform vertical oscillations, but for only 10 to 20 cycles (depending on the perfection of the initial vertical displacement), and it will then undergo a complicated maneuver leading to nearly pure horizontal oscillations with twice the amplitude of the original vertical oscillations. The bob then quickly reverses this process and returns to the vertical oscillation mode, thereby completing a "transfer cycle". This cycle repeats itself over and over with a period which is usually less than 30 sec. To convince a knowledgeable observer that this coupling action cannot result from a linear resonance, it need only be pointed out that both the period and the amplitude of the horizontal oscillations are twice those of the vertical oscillations during a transfer cycle. To demonstrate that this phenomenon does not result from some peculiarity of the spring, it is only necessary to detune the system out of resonance. This can be readily accomplished by lengthening the supporting cord so that L is increased by about 30%; after this change has been made, the bob will execute vertical oscillations with monotonous regularity.

Close observation of the resonant elastic pendulum will reveal the following specific properties of the transfer cycle. (1) The speed with which the energy transfers from one mode to the other is proportional to the initial vertical displacement. (2) The more perfectly the initial displacement is vertical, the longer will be the time required for the energy transfer to the horizontal mode, and the more nearly complete will be this energy transfer. (3) The system spends a longer time in the vertical mode than in the horizontal mode. (4) If the system is not exactly at resonance, this defect will be apparent only for a small initial displacement, and will be almost unnoticeable for large displacements. These properties will be explained later.

The vertical and horizontal oscillations constitute the normal modes of the system as defined by the linear theory. At resonance, only a perfectly vertical oscillation will persist indefinitely (except for the limitations of the uncertainty principle); however, this eigenstate is unstable since even a minute disturbance will induce a transfer cycle. Moreover, horizontal oscillations of finite amplitude are always unstable at resonance. The system does, however, possess two completely stable periodic modes for a given total energy, which correspond to unique parabolic trajectories for the pendulum bob. As will be seen, these

stable periodic modes furnish an interesting subject for a combined theoretical and experimental study.

The coupling action of the resonant elastic pendulum bears a superficial resemblance to the "pumping" of a child's swing.[4] However, the swing pumping phenomenon can be explained within a linear theory since it represents an example of the parametric resonance.

II. DESCRIPTION OF TRANSFER CYCLE

Before proceeding with the analysis, we shall present a qualitative description of the detailed motion of the pendulum bob during a transfer cycle. For this purpose, we have made use of the XDS Sigma-7 computer in the cyclotron laboratory, which is equipped with a Cal-comp plotter as one of its output options. Using this facility, the equations of motion for the pendulum bob can be integrated numerically, and the resultant trajectory can be plotted directly as part of the output. One of these plots, which reveals the nature of the transfer cycle, is shown in Fig. 2.

The trajectory of the pendulum bob during a transfer cycle has two characteristic subsections, and to illustrate this fact, the plot of Fig. 2 has been divided into two diagrams. The scales shown in these diagrams are in units of L, and although the horizontal and vertical scales in the

lower diagram have the correct relative proportion, the horizontal scale in the upper diagram has been magnified by a factor of five in order to reveal the details of the horizontal motion in this part of the transfer cycle. The bob starts from rest at the point labelled 0 in the upper diagram, and the sequence of numbers (1 to 7 in the upper diagram, and 8 to 15 in the lower diagram) indicate the successive low points in the ensuing oscillations. The trajectory shown in the upper diagram is continued without any break in the lower diagram; the last point in the upper diagram, which is marked by an arrow following the number 7, corresponds to the beginning point near the origin of the lower diagram, with an arrow shown for guidance just beyond this point. The trajectory terminates following the number 15 at the point labelled P, where the bob is once again instantaneously at rest. If the trajectory were continued from the point P, the bob would then retrace the exact same path backwards to the starting point 0 in the upper diagram, thereby completing the transfer cycle.

The complex structure of the trajectory shown in Fig. 2 can be greatly simplified if we recognize that the motion proceeds through a sequence of Lissajous figures whose parameters change slowly in the course of the motion. If the vertical and horizontal displacements are denoted by

x and y, respectively, then (as will be shown in the next section) the solutions of the purely linear oscillation equations can be written in the following form:

$$x = A \cos(\omega_x t+\phi), \tag{3a}$$

$$y = 2B \cos(\omega_x t/2), \tag{3b}$$

where the amplitudes A and B, and the relative phase ϕ are all constants. We have assumed that $\omega_x = 2\omega_y$, and the above equations therefore define the set of closed Lissajous figures characteristic of this frequency relationship. For $\phi = 0$ or π, these figures are parabolas, while for $\phi=\pm\pi/2$, they become "infinity-shaped" figures. If we calculate the energies of the vertical and horizontal linear oscillations using the above equations, then we find that $(A/B)^2$ gives the ratio of these energies. As will be shown in Sec. V, the small nonlinear coupling forces may alter this ratio, but will leave the sum of these energies approximately constant. The trajectory of the pendulum bob may therefore be considered instantaneously as a Lissajous figure characterized by particular values of A, B, and ϕ, with the nonlinear forces then serving to produce slow changes in the parameters (A/B) and ϕ, while leaving the sum $A^2 + B^2$ unchanged. In effect, the motion can then be described through the slow variation of the relative phase ϕ and one of the amplitudes, say A.

The upper diagram of Fig. 2 shows the part of the transfer cycle which we shall refer to as the "temporizing mode"

since the value of A remains nearly constant during this part of the cycle. At the starting point 0, the displacements are: $x = 0.100$ and $y = 0.014$. These displacements yield: $(A/B)^2 \simeq 200$, so that the vertical oscillations initially contain about 99.5% of the total energy. Although the horizontal amplitude increases continuously during this part of the cycle, this increase remains relatively insignificant since less than 5% of the energy is transferred here. However, an important change does occur in the relative phase ϕ. The initial Lissajous figure is a parabola corresponding to the value $\phi = 0$, and as the motion proceeds, the value of ϕ moves toward $-\pi/2$, so that the Lissajous figure evolves toward one which is infinity-shaped and centered at the origin.

The lower diagram of Fig. 2 illustrates the part of the transfer cycle which we shall call the "pumping mode", since energy is pumped from the vertical to the horizontal oscillations in a manner which is quite similar to the pumping action of a child's swing. Here, the amplitude A of the vertical oscillations decreases rapidly while the phase ϕ remains close to the optimum pumping value, $\phi = -\pi/2$, during most of this segment of the cycle. Consequently, the Lissajous figure retains an infinity-like shape while proceeding from a tall and narrow figure toward a short and broad figure. On the last swing, when the vertical

oscillation energy has almost been depleted, there is a sudden change in ϕ so that the trajectory ends at the point P with $\phi = -\pi$. At the end point P, the displacements are: $x = -0.015$ and $y = 0.200$, so that $(A/B)^2 \approx 0.02$ here. The horizontal oscillations therefore contain about 98% of the energy at this point, so that a fairly complete transfer of energy has occurred during this half of the cycle.

Although the trajectory displayed in Fig. 2 contains all of the typical features of one half of a transfer cycle, it is somewhat unique in one respect. This uniqueness lies in the fact that the maximum horizontal displacement occurs at the point P where the vertical velocity component (as well as the horizontal one) is simultaneously equal to zero. This result, which makes the two halves of the transfer cycle perfectly symmetric, was sought out on purpose only because it greatly simplified our presentation of these phenomena. In addition, an initial displacement of about twice the normal size was employed in order to speed up the transfer cycle sufficiently so as to avoid an overcrowding of the lines in Fig. 2. In should be noted that in the second half of the transfer cycle, where the bob retraces its path from the point P back to the initial point O, the values of ϕ take on positive rather than negative values, as can be shown by applying time reversal arguments to Eq. (3). The qualitative discussion of the transfer cycle presented in

this section does not account for the observed systematic changes in A and ϕ, and such an accounting will be developed in the succeeding sections.

III. EQUATIONS OF MOTION

We treat the motion of the system as a one-body problem consisting of a mass m moving under the action of a conservative potential energy function V. The motion is assumed to occur in a plane, and the cartesian coordinates X and Y are employed to denote, respectively, the vertical and horizontal displacements of the mass m from equilibrium, with the +X direction being vertically downward. We ignore any nonlinearity in the spring itself, and take V(X,Y) to have the following simple form:

$$V = -mg'X + \tfrac{1}{2}k(r - L_o)^2, \tag{4}$$

where: $r^2 = (L + X)^2 + Y^2$, (4a)

and where g', L_o, and L are defined in Eqs. (1a-c).

The notation can be simplified by expressing the energy of the system in units of kL^2, and by introducing the following dimensionless variables:

$$x = X/L,\ y = Y/L,\ \lambda = L_o/L, \tag{5}$$

where: $0<\lambda<1$. In terms of these variables, the function V takes on the following form:

$$V = \tfrac{1}{2}(x^2 + y^2) - \lambda\left\{[(1+x)^2 + y^2]^{1/2} - (1+x)\right\}, \tag{6}$$

where we have dropped the constant term in order to make:

$V = 0$ at equilibrium. Since both x and y will be restricted to small numbers, the function V may justifiably be expanded in powers of these variables; such an expansion leads to the following result:

$$V = V_o + V_1, \tag{7}$$

$$V_o = \frac{1}{2}[x^2 + (1-\lambda)y^2], \tag{7a}$$

$$V_1 = \frac{1}{2}\lambda[xy^2 - x^2y^2 + (1/4)y^4], \tag{7b}$$

where V_o characterizes the linear oscillations, and where V_1 contributes the nonlinear forces acting on these oscillations. The expression (7b) for V_1 contains all the cubic and quartic terms from the expansion, but omits all the higher order terms; however, this truncated form for V_1 is quite sufficient for our purposes here. The cubic term in V_1 plays the dominant role in providing the driving force responsible for the $\omega_x = 2\omega_y$ coupling resonance phenomena, so that even the quartic terms can often be safely neglected.

Rather than using the time t as the independent variable, we introduce for this purpose the angle θ which is given by:

$$\theta = \omega_x t, \tag{8}$$

with ω_x defined by Eq. (1); in addition, we shall use primes on the dependent variables to designate derivatives with respect to θ. Using the dimensionless variables defined above, we then obtain the following equations of motion for the system:

$$x'' + x = f_x, \tag{9a}$$

$$y'' + (1-\lambda)y = f_y, \tag{9b}$$

where f_x and f_y are the nonlinear force components derived exclusively from V_1, and consequently given by:

$$f_x = -\tfrac{1}{2}\lambda y^2(1-2x), \tag{10a}$$

$$f_y = -\lambda y(x-x^2 + \tfrac{1}{2}y^2). \tag{10b}$$

In the linear approximation where f_x and f_y are both zero, the x and y oscillations are uncoupled so that these coordinates constitute the normal modes for the system. In this case, ω_x and ω_y of Eq. (1) give the corresponding angular frequencies of these oscillations, and these frequencies are related as follows:

$$\omega_y = q\omega_x, \; q = (1-\lambda)^{1/2}, \tag{11}$$

and since $0<\lambda<1$, it follows that: $\omega_y<\omega_x$. The values $\lambda = 3/4$ and $q = 1/2$ are of special interest here since they correspond to the frequency relation: $\omega_x = 2\omega_y$ for which the resonance coupling action is observed.

In terms of the dimensionless units introduced above, the kinetic energy T of the system is given by:

$$T = \tfrac{1}{2}[(x')^2 + (y')^2]. \tag{12}$$

If H denotes the Hamiltonian for the system, and if E is the total energy, then we may write:

$$H = T + V = E, \tag{13}$$

where V is given by Eq. (7). The momenta p_x and p_y, which

are conjugate to the coordinates x and y, are then evidently given by:

$$p_x = x', \; p_y = y', \tag{14}$$

and the canonical equations of motion reduce, as they must, to those given in Eqs. (9,10).

As mentioned in the previous section, a computer program is available which provides information about the motion of the pendulum bob. This program integrates numerically the specific equations of motion (9,10) above, and the accuracy of the results is therefore limited by the approximate nature of these equations. Further results from this program will be presented later.

IV. NONLINEAR RESONANCE CONDITION

As is well known, a resonance condition will be produced in an oscillator when it is driven by a periodic force having the same frequency. Considering only the lowest order (quadratic) terms in f_x and f_y of Eq. (10), we observe that f_x varies as y^2 and that f_y varies as xy. These forces are treated as small perturbations acting on the linear x and y oscillations. Since these oscillations have frequencies ω_x and ω_y, respectively, then f_x has component frequencies: $2\omega_y$ and 0, while f_y has component frequencies: $\omega_x \pm \omega_y$. We therefore find that f_x and f_y will both have components with the proper resonant frequencies provided:

$\omega_x = 2\omega_y$. This then is the resonant frequency condition for the cubic term in V_1 to be effective in coupling the two linear oscillation modes.

An equivalent but simpler derivation of the resonance condition can be obtained from the nonlinear force potential V_1 of Eq. (7b). As will be shown in the next section, a given V_1 will produce a significant perturbation only if it fulfills the condition:

$$\langle V_1 \rangle = 0, \tag{15}$$

where the averaging is performed over the unperturbed linear oscillations. Considering only the cubic term in Eq. (7b), that is: V_1 varies as xy^2, this condition then yields directly: $\omega_x = 2\omega_y$, which is the same result found above.

It seems worthwhile to digress here in order to point out that the nonlinear resonance condition can also be derived from the perturbation theory of quantum mechanics.[5] If the two dimensional linear oscillator is quantized, then the energy eigenvalues are given by:

$$E(n_x,n_y) = (n_x + \tfrac{1}{2})\hbar\omega_x + (n_y + \tfrac{1}{2})\hbar\omega_y, \tag{16}$$

where the quantum numbers n_x and n_y take on the values: 0,1,2,.... If we consider the transition: $n_x \to n_x'$, $n_y \to n_y'$, then the transition probability will be insignificantly small unless the following two conditions are satisfied:

$$E(n_x,n_y) = E(n_x',n_y'), \tag{17a}$$

$$(n_x,n_y|V_1|n_x',n_y') \neq 0, \tag{17b}$$

where the latter represents the matrix element of the perturbation V_1 between the states in question. The first of these conditions yields:

$$(n_x' - n_x)\omega_x = -(n_y' - n_y)\omega_y. \tag{18a}$$

If we take, as before, $V_1 \sim xy^2$, then the second condition (17b) leads to the following selection rules:

$$n_x' - n_x = \pm 1;\ n_y' - n_y = 0, \pm 2. \tag{18b}$$

It then follows that both conditions can be satisfied only if: $\omega_x = 2\omega_y$, which is identical to the result of the classical theory found above.

The quartic terms in V_1 of Eq. (7b) do not excite any nonlinear coupling resonances in this system where $\omega_y < \omega_x$. These terms do, however, produce a significant shift in the frequencies of the x and y oscillations for large amplitudes, and can therefore serve to limit the effect of nonlinear resonances. Among the higher order terms omitted from V_1, the quintic term which varies as xy^4 would (by extension of the arguments given above) produce resonant coupling action when $\omega_x = 4\omega_y$; however, the frequency shifting capability of the quartic terms prevents this resonance from exhibiting a significant effect except at unreasonably large amplitudes. Although the xy^2 term is mainly responsible for driving the $\omega_x = 2\omega_y$ resonance, the xy^4 and x^3y^2 terms in V_1 will also contribute to this resonance, and the contribution from these quintic terms

can safely be neglected only for small amplitudes. The procedures used in this section can be generalized to encompass the nonlinear resonance conditions for other systems.

V. PERTURBATION THEORY

As is customary in perturbation calculations, we start with the exact solutions of the unperturbed linear oscillation equations (9). These solutions are written in the following form:

$$x = A\cos(\theta+\alpha), \tag{19a}$$

$$y = 2\kappa B\cos(q\theta+\beta_o), \tag{19b}$$

where A, α, κ, B and β_o are all constants, and where q is defined in (11). We have introduced the extra constant κ here in order to simplfy our results later on; with this in mind, we specifiy that:

$$\kappa = (2q)^{-1/2}. \tag{19c}$$

It should also be noted that when the resonance condition $q=\frac{1}{2}$ obtains, then $\kappa=1$, and the above solutions closely resemble those given in (3) provided we take: $\phi = \alpha-2\beta_o$. The analysis now proceeds to investigate how the nonlinear force potential V_1 of Eq. (7b), treated as a perturbation, affects the otherwise constant amplitudes and phases of these oscillations.

Although it is quite feasible to work through the perturbation calculation using the differential equations (9,10), we shall utilize instead the Hamiltonian and canonical transformation technique.[6] The two methods must obviously yield the same results, but the Hamiltonian method possesses real elegance and serves to confirm the appropriateness of the adjective "canonical". Corresponding to the above solutions for the linear oscillation equations, the momenta p_x and p_y of Eq. (14) are given by:

$$p_x = -A \sin(\theta+\alpha), \tag{20a}$$

$$p_y = -2q\kappa B \sin(q\theta+\beta_o). \tag{20b}$$

We now transform the problem to a new set of canonical variables which are closely related to the familiar "angle and action variables".[7] The coordinates x and y are replaced by the phase angles α and β, where α is given in (19a,20a), and where β is defined by:

$$\beta = (q-\tfrac{1}{2})\theta+\beta_o, \tag{21}$$

so that the argument $(q\theta+\beta_o)$ in (19b,20b) now becomes: $(\frac{1}{2}\theta+\beta)$; this change in argument will simplfy our calculations later on. It also proves convenient to introduce the "off-resonance" parameter δ which we define by:

$$\delta = q - \tfrac{1}{2}. \tag{21a}$$

With κ specified by (19c), the action variables p_α and p_β are then given by:

$$p_\alpha = \frac{1}{2}A^2, \; p_\beta = B^2; \tag{22}$$

with these definitions, the transformations: $x, p_{x\to\alpha}, p_\alpha$ and $y, p_{y\to\beta}, p_\beta$ are then canonical. In the absence of any perturbation, the new variables evidently satisfy the following differential equations: $p_\alpha' = p_\beta' = \alpha' = 0$, and $\beta' = \delta$, as follows from (21).

The generating function $G(x,\alpha,y,\beta,\theta)$ for the above transformation is specified by:[7]

$$G = -\frac{1}{2}x^2 \tan(\theta+\alpha) - \frac{1}{2}qy^2 \tan(\tfrac{1}{2}\theta+\beta), \tag{23}$$

since, as follows from (19-22) above, it satisifies the equations:

$$p_x = (\partial G/\partial x), \; p_\alpha = -(\partial G/\partial \alpha), \tag{23a}$$

together with the corresponding equations for p_y and p_β. As a result, when the Hamiltonian H of Eq. (13) is transformed to the new variables, the new Hamiltonian $H^*(\alpha,\beta,p_\alpha,p_\beta,\theta)$ is then found to be:

$$H^* = H+(\partial G/\partial\theta) = (\delta)p_\beta + V_1(\alpha,\beta,p_\alpha,p_\beta,\theta), \tag{24}$$

where V_1 here is obtained by inserting Eqs. (19-22) into Eq. (7b). This new Hamiltonian depends explicitly on θ, and is therefore not a constant of the motion. We now have the following equations of motion for the system:

$$p_\alpha' = -(\partial V_1/\partial\alpha), \; \alpha' = (\partial V_1/\partial p_\alpha); \tag{24a}$$

$$p_\beta' = -(\partial V_1/\partial\beta), \; \beta' = \delta + (\partial V_1/\partial p_\beta). \tag{24b}$$

Since no approximations have yet been introduced, these equations of motion are exact.

Considering only its explicit dependence on θ, the function V_1 of Eq. (24) can be expressed as a Fourier series having the fundamental period: $\Delta\theta = 2\pi$. The oscillatory part of V_1 will produce small fluctuations in the angle and action variables which are of no real consequence. If, however, V_1 contains terms which are nonoscillatory, then such terms will produce systematic changes in these variables, and it is only such changes which have real importance. The perturbation calculation therefore proceeds to eliminate the insignificant fluctuations by replacing V_1 in the equations of motion (24) by its average value: $V_1 \rightarrow \langle V_1 \rangle$, where the average is taken over θ assuming that the other variables remain constant. This procedure corresponds to a "first order" perturbation treatment, which is as far as we shall carry the problem. The equations of motion are therefore derived from a Hamiltonian $K(\alpha,\beta,p_\alpha,p_\beta)$ which is given by:

$$K = (\delta)p_\beta + \langle V_1 \rangle. \tag{25}$$

Since this Hamiltonian K does not depend explicitly on θ, it therefore represents an approximate constant of the motion for the system.

After averaging V_1 of Eq. (24) over θ, we then obtain the following expression for the invariant K:

$$K = B^2[\delta+\mu(A\cos\phi-A^2+\mu'B^2)], \tag{26}$$

where ϕ, μ, and μ' are given by:

$$\phi = \alpha - 2\beta, \tag{26a}$$

$$\mu = \frac{1}{2}\lambda\kappa^2 = (1 - q^2)/(4q), \qquad \mu' = (3/2)\kappa^2 = 3/(4q), \tag{26b}$$

as a consequence of the definitions (11,19c). We have chosen to retain A and B in this expression for K since these amplitudes represent more familiar concepts than the action variables p_α and p_β given by (22). Since this K depends on α and β only through the quantity ϕ, it follows that:

$$2p_\alpha' + p_\beta' = -2(\partial K/\partial\alpha) - (\partial K/\partial\beta) = 0. \tag{27a}$$

We therefore have an additional (approximate) invariant C, which is given by:

$$2p_\alpha + p_\beta = A^2 + B^2 = C^2, \tag{27b}$$

where we have used (22). The invariance of C can also be derived from the total energy E of the system, which is a true constant of the motion. Thus, when Eq. (13) is averaged over θ, we find:

$$E = \langle H \rangle = \frac{1}{2}C^2 + K, \tag{28}$$

So that the invariance of E and K implies the invariance of C.

Returning to the Hamiltonian $K(\alpha,\beta, p_\alpha,p_\beta)$ of Eqs. (25,26), and expressing the canonical equations of motion in terms of A and B, we then obtain:

$$A' = -A^{-1}(\partial K/\partial\alpha) = \mu B^2 \sin\phi, \tag{29a}$$

$$\alpha' = 2(\partial K/\partial A^2) = \mu(B^2/A)(\cos\phi - 2A), \tag{29b}$$

$$\beta' = (\partial K/\partial B^2) = \delta + \mu(A\cos\phi - A^2 + 2\mu' B^2), \tag{29c}$$

which follow from Eq. (22). We have omitted the corresponding equation for B' since the invariant C of Eq. (27b) makes this equation superfluous. It may be observed that only the cubic term in V_1 contributes to A', and hence, to the exchange of energy between the vertical and horizontal oscillation modes. The quartic terms in V_1 affect only α' and β', and these derivatives correspond to frequency shifts in the oscillation modes, as mentioned in the preceding section. In order for the results obtained in this section to be valid, the phases and amplitudes of the oscillations must remain nearly constant within a period: $\Delta\theta = 2\pi$, and this condition can be satisfied provided we consider only small values of δ, and provided we also limit the amplitudes so that: $C \lesssim 0.1$. The latter limitation is also required to justify the truncation of the power series for V_1 given in Eq. (7b).

A. Modified Lissajous Figures

With the two invariants K and C at our disposal, we can reduce the problem to the two variables A and ϕ. Using Eq. (27b) to eliminate B, then K of Eq. (26) reduces to:

$$K = (C^2 - A^2)[\delta + \mu(A\cos\phi - A^2 + \mu'(C^2 - A^2))]. \qquad (30)$$

The invariant $K(A,\phi)$ may now be considered as the Hamiltonian involving the coordinate ϕ and its conjugate momentum: $p_\phi = \frac{1}{2}A^2$. The differential equations of motion for these

variables are therefore given by:

$$A' = -A^{-1}(\partial K/\partial\phi); \quad \phi' = A^{-1}(\partial K/\partial A). \tag{31}$$

These equations can be verified by comparison with Eqs. (29a-c) and by recalling that: $\phi'=\alpha'-2\beta'$ from Eq. (26a).

The solutions (19) can be reformulated in terms of the variables A and ϕ as follows:

$$x = A\cos(\theta+\phi), \tag{32a}$$

$$y = 2\kappa(C^2-A^2)^{1/2}\cos(\theta/2), \tag{32b}$$

where we have set:

$$\theta = \theta+2\beta(\theta), \tag{32c}$$

and where we have used Eqs. (21,27b). If θ is considered as the independent variable, then these equations define the set of Lissajous figures characteristic of the frequency ratio 2:1, and the form of these figures is specified entirely by the two parameters A and ϕ. As long as the system is close to resonance, the trajectory of the pendulum bob will correspond to a Lissajous figure which modifies its form slowly as the parameters A and ϕ undergo adiabatic changes. When the system is exactly at resonance, the relations $\delta=0$ and $\kappa=1$ obtain, and these trajectory equations become equivalent to those given in Eq. (3), except for the slight variation in β resulting from the nonlinear forces.

VI. INVARIANT CURVES

A particular trajectory for the pendulum bob will be characterized by specific values for the (approximate) constants K and C, as determined by the initial conditions. This trajectory will evolve in accordance with the variations of the parameters A and ϕ from their initial values. However, because Eq. (30) for K provides a specific relationship between these variables, the nature of this trajectory will therefore be completely determined except for its time dependence. The A versus ϕ curve resulting from Eq. (30) for given values of K, C and δ is known as an "invariant curve", and it is customary to plot such curves by treating (A,ϕ) as a set of plane polar coordinates. A set of invariant curves is obtained by assuming fixed values for C and δ, and considering all possible constant values for K. Such sets of invariant curves provide complete information in a compact format on the possible types of trajectories for the pendulum bob.

To simplify the discussion, we shall omit the quartic terms in K so that Eq. (30) reduces to:

$$K = \mu(C^2 - A^2)(\varepsilon C + A\cos\phi), \tag{33}$$

where we have set:

$$\varepsilon = \delta/(\mu C). \tag{33a}$$

Although the omission of the quartic terms is fully justified only for small C values, it is just such cases which require

our closest attention since we wish to demonstrate that the resonance coupling action will occur even for small amplitudes. Moreover, within the restriction: $C \lesssim 0.1$ noted above, the quartic terms in K do not modify appreciably the results derived in this section. The equations of motion corresponding to (31) now reduce to:

$$A' = \mu(C^2 - A^2)\sin\phi, \tag{34a}$$

$$\phi' = -2\mu\varepsilon C + \mu[(C^2 - 3A^2)/A]\cos\phi. \tag{34b}$$

In presenting sets of invariant curves, such as those shown in Fig. 3 and Fig. 4, we have employed a set of dimensionless variables (u,v) defined by:

$$u = (A/C)\cos\phi, \quad v = (A/C)\sin\phi. \tag{35}$$

When expressed in terms of these variables, the function K of (33) depends on C only as a scale factor. With the quartic terms in K omitted, we therefore find that the off-resonance parameter ε completely determines the geometry of the set of invariant curves.

The set of invariant curves shown in Fig. 3 is obtained when the system is exactly at resonance, that is, when $\varepsilon=0$. The K=0 curve consists of the bounding circle: A=C, together with the straight line: $\phi=\pm\pi/2$, A<C, which divides the diagram into two symmetric configurations, and is therefore referred to as a "separatrix". This K=0 curve consequently contains those points which represent pure vertical motion (A=C) as well as the point representing

pure horizontal motion (A=0). The function K has two saddle points located at:

$$u = 0, \quad v = \pm 1, \tag{36a}$$

located on the K=0 curve; these points are referred to as "unstable fixed points". Furthermore, the function K has its maximum and minimum values at the two isolated points shown in the diagram whose coordinates are:

$$u = \pm(1/3)^{1/2}, \; v = 0; \tag{36b}$$

these points are referred to as "stable fixed points". (The trajectories corresponding to these stable fixed points will be discussed at length in Sec. VIII.) At all four of these fixed points, the equations: $A'=\phi'=0$ hold, as follows from (34). The arrows shown in Fig. 3 and Fig. 4 indicate the direction of motion for the points on these curves as time increases; the proper direction for these arrows follows immediately from (34).

The invariant curves in Fig. 3 with $|K| \simeq 0$ have a pronounced "D" shape, and these curves provide a good explanation for the existence of the "transfer cycle". If the bob is displaced vertically downward, but not perfectly so, then its initial state corresponds to $A \simeq C$ and its corresponding invariant K value will therefore be quite small. The motion of the bob will correspond initially to a point in the diagram lying on the semicircular portion of the D. As time passes, this point proceeds around the semicircle until

it reaches the "corner" of the D near $\phi=-\pi/2$; it then turns the corner and proceeds up along the straight line portion of the D, and as it passes by the origin, the motion of the bob will be nearly horizontal ($A\simeq 0$). The representative point then continues up the straight line and back around to its starting position, thereby completing the transfer cycle. The systematic changes in A and ϕ described in Sec. II have now been accounted for.

Having established a basis for understanding the resonance coupling action observed in the elastic pendulum, it remains to be shown that this action disappears when the system is out of resonance. This can be most readily accomplished by considering the set of invariant curves obtained from (33) when $\varepsilon\neq 0$. The invariant curve for K=0 again contains the bounding circle: A=C, but the straight line portion of this curve is now given by: $u=-\varepsilon$. For $|\varepsilon|<1$, the two unstable fixed points will now have the coordinates:

$$u = -\varepsilon, \quad v = \pm(1-\varepsilon^2)^{1/2}. \tag{37a}$$

Moreover, the two stable fixed points have the following new set of coordinates:

$$3u = -\varepsilon\pm(3+\varepsilon^2)^{1/2}, \quad v = 0, \tag{37b}$$

so that as $|\varepsilon|$ increases, one of these points will move toward the origin, while the other moves towards the bounding circle. For $|\varepsilon|=1$, the latter point and the two unstable

fixed points will all coalesce at the single point: $u=-\varepsilon$, $v=0$, on the bounding circle. These phenomena are illustrated in Fig. 4 which contains two sets of invariant curves, one for $\varepsilon=0.5$, and the other for $\varepsilon=1.0$. When $|\varepsilon|>1$, the invariant curve diagram is then characterized by a single stable fixed point; in this case, the vertical oscillation mode will be completely stable. Thus, the resonance coupling action will effectively disappear when: $|\delta|>\mu C$, as follows from (33a). On the other hand, for a given value of the off-resonance parameter δ, the resonance coupling action can always be induced simply by increasing the initial oscillation amplitude sufficiently so as to make: $C>>|\delta|/\mu$.

A. Phase Space Plots

The motion of the pendulum bob can be represented by a curve traced out in the four dimensional (x,p_x,y,p_y) phase space associated with this system. If we consider only those points along this curve for which $y=0$, it then follows from (32,20,35) that: $\Theta=\pm\pi$, and that x and p_x are given by:

$$x = -A\cos\phi = -uC,\quad p_x = A\sin\phi = vC. \tag{38}$$

As the motion proceeds, a two dimensional plot of these particular (x,p_x) points will form a trajectory which will presumably coincide with one of the invariant curves

discussed above. Such (x,p_x) phase space plots will therefore provide a convenient method for comparing the results of the analysis with computer output data on the motion of the system.

Fig. 5 presents a set of p_x versus x phase space plots obtained by numerical integration of Eqs. (9,10) with $\lambda=3/4(\delta=\varepsilon=0)$, and with initial conditions chosen so that in each case: C = 0.05. These curves were generated by the following set of initial conditions: $y=0$, $p_x=0$, $x=\pm 0.98C$, $\pm 0.9C$, $\pm 0.75C$, and with the corresponding values of p_y obtained from: $p_y^2=2E-x^2$, where E is calculated from (28) using the K value from (30). (It should be noted that these curves all have the same C value, but not the same E value.) Consequently, the initial points on all these curves lie on the x axis. The succeeding (x,p_x) values plotted in this figure were printed out by the computer each time the condition y=0 was satisified; actually, only every other point $(\Delta\theta=4\pi)$ was plotted in order to avoid an overcrowding of the points. In order to show each point distinctly, these plots were terminated before they actually closed. The two stable fixed points which are shown in Fig. 5 were computed by a procedure described in Sec. VIII.

The particular set of invariant curves plotted in Fig. 3 were obtained by choosing those curves which passed through the points: $v=0$, $u=\pm 0.98$, ± 0.9, ± 0.75, so that

these curves should correspond exactly with those shown in Fig. 5. Indeed, when the two separate sets of curves (plotted on semi-transparent paper with the same scale) are superimposed, they coincide precisely to within the plotting accuracy. Moreover, when the plots of Fig. 5 are continued beyond the termination points actually shown, the succeeding (x,p_x) points repeatedly fall on their respective invariant curves with the same degree of accuracy. An examination of the actual numerical data shows that the absolute disagreement between the computer data and the analysis does not exceed about 0.01C. This disagreement will, however, increase rapidly with the value of C.

VII. TRANSFER CYCLE PERIODS

Quantitative information on the time required to complete a transfer cycle can be obtained from the computed phase space plots of Fig. 5 simply by counting the points around the corresponding invariant curve. If N is the number of vertical oscillation periods required to complete a transfer cycle, then an application of dimensional arguments to Eq. (34) yields:

$$N = (\Delta\theta)/2\pi \sim (\mu C)^{-1}, \tag{39}$$

so that the rate at which a transfer cycle is traversed is proportional to C. The calculation of N will be carried

out only for the case of exact resonance, and with the quartic terms in K once again being neglected. The invariant K is therefore given by (33) with $\varepsilon=0$, and the differential equations (34) will apply here. We shall restrict our attention to those cases where the pendulum bob has an initial displacement which is almost perfectly vertical, so that the relevant invariant curves are those having the pronounced D shape in Fig. 3, and which result from: $|K|\simeq 0$. Such cases correspond to the transfer cycle in its most characteristic form.

The semicircular portion of the invariant curve, which corresponds to the "temporizing mode" of the transfer cycle, is characterized by a nearly constant A value: $A\simeq C$. If we make the approximation that $A=C$, then Eq. (34b) for ϕ' can be readily integrated, and the following result is obtained:

$$\tan(\phi/2) = -\tanh(\mu C\theta), \tag{40a}$$

where we have set: $\phi=0$ at $\theta=0$, and where θ ranges from $-\theta_1$ to $+\theta_1$. The nearly straight-line portion of the invariant curve, which corresponds to the "pumping mode" of the transfer cycle, is characterized by: $\phi\simeq\pm\pi/2$. Under this condition, integration of (34a) for A' then leads to the result:

$$A(\theta) = C|\tanh(\mu C\theta)|, \tag{40b}$$

where we have assumed: $\phi=\pm\pi/2$, and $A(0)=0$, and where θ

ranges from $-\theta_2$ to $+\theta_2$. After we have determined θ_1 and θ_2, then the value of N is given by: $N = (\theta_1+\theta_2)/\pi$, since $\Delta\theta = 2(\theta_1+\theta_2)$ obtains for the complete cycle.

We consider now the behaviour of the invariant curve in the vicinity of the two unstable fixed points whose coordinates are: $A=C$, $\phi=\pm\pi/2$, as given in (36a). After setting: $A=C-\delta A$, and $\phi=\pm(\frac{1}{2}\pi-\delta\phi)$, then K of (33) reduces to:

$$K = 2\mu C^2(\delta A)(\delta\phi), \tag{41}$$

when only the lowest order term in δA and $\delta\phi$ is retained. The point on this hyperbolic curve which comes closest to the fixed point has the following coordinates:

$$\delta\phi = (\delta A)/C = s, \tag{41a}$$

where s is a parameter defined by: $K = 2\mu C^3 s^2$. If the motion starts at some point (A_o,ϕ_o) on the invariant curve, then the value of s can be calculated from:

$$(C^2-A_o^2)A_o|\cos\phi_o| = 2C^3s^2, \tag{41b}$$

which results from a comparison of (33) with (41).

We can now calculate the values of θ_1 and θ_2 in terms of the parameter s by recognizing that the limiting values of ϕ and A on the two separate portions of the invariant curve are given by:

$$\phi(\theta_1) = -(\tfrac{1}{2}\pi-s),\ A(\theta_2) = C(1-s), \tag{42a}$$

as follows from (41a). Inserting these values into (40a,b), we then find:

$$1-s = \tanh(\mu C\theta_1) = \tanh(\mu C\theta_2), \tag{42b}$$

where we have retained only the first order term in s in order to preserve consistency with our previous approximations. Since this result implies that $\theta_1 = \theta_2$, we must therefore conclude that the pendulum bob spends an approximately equal amount of time in the temporizing mode and in the pumping mode of a transfer cycle. This conclusion is confirmed by the computer data presented in Fig. 2 and in Fig. 5.

Since the parameter s is quite small, the hyperbolic tangent in (42b) can be replaced by its asymptotic form, so that:

$$\theta_1 = \theta_2 = (2\mu C)^{-1} \ell n(2/s). \tag{43a}$$

We therefore obtain the following expression for N:

$$N = (\theta_1 + \theta_2)/\pi = (\pi\mu C)^{-1} \ell n(2/s), \tag{43b}$$

with the parameter s determined from (41b). If we take as an example the two phase space plots of Fig. 5 with initial conditions: A_o=0.98C, ϕ_o=0 and π, then the computer output yields the value: N=45.2 in both cases; for the same initial conditions, the above formulas yield: s=0.139 and N=45.3, which agrees very well with the computer result. For the case discussed in Sec. II, where $\phi_o = 0$ and $(A_o/C)^2 = 0.995$, the computer result is: N=31.5, while the above formulas yield: s=0.05 and N=31.3; this agreement indicates that the quartic terms have an insignificant effect on N even for C = 0.1.

VIII. STABLE PERIODIC MODES

The two stable fixed points mentioned above (cf. (36b)) and shown in Fig. 3 imply the existence of two stable periodic modes of motion for a given total energy E. Each of these fixed points represents a state in which the pendulum bob repeatedly executes a fixed parabolic trajectory, with the parabola standing "nose-up" in one case, and "nose-down" in the other. In calculating the properties of these trajectories, we shall retain the quartic terms in K of (26) and the differential equations (29). We shall, however, restrict the discussion to the case of exact resonance, although these fixed point trajectories may exist even when the system is out of resonance (cf. (37b) and Fig. 4). Since $\delta=0$ will prevail here, the values of κ, μ, and μ' of (19c,26b) are given by: $\kappa=1$, $\mu=3/8$, $\mu'=3/2$.

The condition $A'=0$ holds for these trajectories, and it follows from (29a) that $\phi=0$ or π. If we eliminate θ from (32a,b), the following equation for the parabolic trajectory is obtained:

$$x = a[2(y/b)^2-1], \tag{44}$$

where we have set: $b=2B$, $a=A\cos\phi = \pm A$, so that $\phi=0$ and $\phi=\pi$ correspond to the nose-up and nose-down configurations, respectively. The properties of these trajectories will

be expressed in terms of $\underline{a}$, since this procedure simplifies the calculations.

In order to relate b and $\underline{a}$, we use the condition: $\phi' = \alpha' - 2\beta' = 0$, which obtains for these trajectories. After combining (29b,c), we finally obtain:

$$b^2 = 8a^2(1-a)/(1-8a). \tag{45}$$

If the quartic terms are omitted, this result reduces to: $b^2=8a^2$, which is equivalent to (36b). In this case, the two parabolas resulting from a given $|a|$ will have the same shape, but the inclusion of the quartic terms removes this symmetry. The values of C and E can now be calculated in terms of $\underline{a}$ by using (27b, 28).

The coordinates: $(x,y)=(a,b)$ specify the position of the bob at the instant when it has zero velocity. Using (32), the time dependence of the trajectory can be written as follows:

$$x = a\cos(2q^*\theta),\ y = b\cos(q^*\theta), \tag{46}$$

where we have set:

$$q^* = \tfrac{1}{2}(d\theta/d\theta) = \tfrac{1}{2} + \beta'. \tag{46a}$$

The angular frequency of these trajectories is therefore: $q^*\omega_x$, and this frequency generally differs from $\omega_y=\frac{1}{2}\omega_x$. To characterize this difference, we introduce the parameter Ω which is defined by:

$$\Omega = 2q^* - 1 = 2\beta'. \tag{47}$$

Using (29c) together with the results found above, we then

obtain: $\Omega=\Omega_1$, where:

$$\Omega_1 = (3/4)a(1-a)(1-2a)/(1-8a), \tag{47a}$$

so that the sign of Ω matches that of $\underline{a}$. When the quartic terms are neglected, this result reduces to: $\Omega=\Omega_o=(3/4)a$. Having derived expressions for the frequency and the shape of these trajectories, all the properties of the stable periodic modes are then specified. Even though the results obtained above include the quartic terms in the perturbation, the accuracy of these results is still limited since they are derived ultimately from a first order perturbation calculation.

The calculation of the properties of the periodic modes can be formulated alternatively as a nonlinear eigenvalue problem, and such a formulation frequently simplifies the calculation. From the symmetry of the trajectories, we recognize that x and y can be expressed as a Fourier series in the following form:

$$x(\theta) = a_o+a_2 \cos(2q^*\theta)+\ldots, \tag{48a}$$

$$y(\theta) = b_1 \cos(q^*\theta)+b_3 \cos(3q^*\theta)+\ldots . \tag{48b}$$

If these expressions are substituted into the differential equations (9,10), the result will be a set of nonlinear algebraic equations relating q^* and the coefficients a_j, b_k; these algebraic equations can then be solved by successive approximations. Another frequently employed

procedure consists of using Hamilton's principle to carry out a variational calculation so as to find the unknown parameters.[8] If, as a first approximation, we assume that all the coefficients in the above series are zero except for a_2 and b_1, then the variational calculation yields the same result as in (45) above, with the identification: $a_2=a$, $b_1=b$; however, we also find that Ω is now given by: $\Omega=\Omega_2$, where:

$$2\Omega_2 + \Omega_2^2 = 2\Omega_1, \tag{49}$$

with Ω_1 given by (47a). In order to achieve still better results, the coefficients a_o and b_3 should also be included in the variational calculation; however, we shall leave this calculation (which can be checked against the computer data provided in Table I) as an exercise for the student.

A. Computer Results

The program which integrates the equations of motion (9,10) was adapted so as to calculate the properties of the stable periodic modes. The program begins at $\theta=0$ with: $x=x_o$, $y=y_o$, $p_x=p_y=0$, and then integrates out to $\theta=\theta_o$ where it tests whether $y=0$ and $p_x=0$ simultaneously; if the test fails, the calculation is iterated with improved values for y_o and θ_o until the test is successfully passed; throughout this process, the value of x_o is held fixed. Having thus found the desired trajectory, the program then calculates the Fourier coefficients a_j and b_k of (48), the

frequency parameter Ω of (47), and the energy E of (13); the last two quantities are obtained from:

$$\Omega = (\pi/\theta_o)-1, \quad E = \tfrac{1}{2}[(x_f)^2 + (p_{yf})^2], \tag{50}$$

where $x=x_f$ and $p_y=p_{yf}$ are the values found at $\theta=\theta_o$.

Table I presents computer output data as a function of x_o. The Fourier coefficients omitted from this table are all quite negligible; for example, the largest of these coefficients (a_4) is less than 0.1% of the value of x_o in all cases. The Fourier series for x and y can therefore be accurately represented by the first two terms shown in (48). The range of admissable x_o values must be limited so that $C<0.1$ (or $E<0.005$), since the equations (9,10) used here will become inaccurate beyond this limit as previously noted. The agreement between the tabulated computer results and the theoretical formulas derived above is quite satisfactory, particularly for small values of $|x_o|$. The magnitudes of a_o and b_3 relative to those of a_2 and b_1 indicate the errors involved in the theoretical formulas. Taking as an example the case where $x_o=0.04$, and making the identification: $x_o=a$, $y_o=b$, we then find from (45): $(b/a)=3.360$, while the computer results yield: $(y_o/x_o)=3.406$.

Fig. 6 presents drawings of the pairs of trajectories which were obtained from the computer program for the energy values: E=1,2, and 5×10^{-3}. The corresponding

parabolic curves specified by the theoretical formulas (44,45) are not shown. The computer trajectories are quite accurately parabolic, since the value of b_3 is so small; however, these parabolas are displaced from the theoretical ones by an amount equal to the value of a_o given in Table I.

Fig. 7 presents a plot of the computed Ω values as a function of x_o. The straight line $\Omega_o=(3/4)x_o$, which is derived from (47a) by setting $x_o=a$ and neglecting the higher order terms, is also plotted in this figure in order to demonstrate the relative importance of these terms. Considering again the $x_o=0.04$ case with the identification: $x_o=a$, we then find: $\Omega_o=0.03$ and $\Omega_1=0.0390$ from (47a), and $\Omega_2=0.0382$ from (49), as compared with the computer value $\Omega=0.0363$ given in Table I. The relative accuracy of these formulas is therefore apparent.

B. Experimental Data

The material presented in Secs. VI(A), VII, and VIII(A) has established that the analytical formulas agree quite well with the computer calculations, and such agreement demonstrates the validity of the mathematical analysis. This agreement does not, however, validate the model upon which the analysis and the computer calculations are both based. Nevertheless, since all the general properties of

the transfer cycle can readily be observed, and since these properties are all predicted by the theory, we must conclude that the theoretical model is at least qualitatively correct. Because of their inherent stability, the periodic modes discussed above provide an excellent framework for quantitative measurements aimed at establishing the validity of the model.

In order to carry out such a measurement, one of the trajectories obtained from the computer output was plotted to the correct scale on a sheet of graph paper, which was then mounted on the wall about one inch behind the pendulum, so that the plotted curve was properly positioned with respect to the center of the bob. The bob was then pulled out to the end point of the plotted curve, where it was released from rest. In all cases where good starting conditions were achieved, the bob was observed to follow the prescribed trajectory with good accuracy for periods of at least 30 oscillations. Releasing the bob properly at the start of its motion often requires several trials. When the bob is improperly released, it will perform small oscillations about the prescribed trajectory, or else its plane of motion will rotate so that it strikes the wall.

The period of these stable oscillations was measured for four trajectories. Three of these correspond to the set of nose-up parabolas shown in Fig. 6, and the fourth

one is the middle member of the set of nose-down parabolas in the same Figure. (The nose-up parabolas are much easier to reproduce accurately since the extra tension of the extended spring facilitates good starting conditions in these cases.) For each trajectory, the time required for 30 oscillations was measured, and this measurement was repeated ten times. Each measurement was restricted to thirty oscillations in order to avoid any significant loss of energy during the measurement. The measured period τ(per cycle) was converted to the corresponding Ω value using the formula: (cf. (47))

$$\Omega = 2(\tau_x/\tau)-1, \tag{51}$$

where: $\tau_x=0.722(7\pm7)$sec is the period of the vertical spring oscillations which was obtained from a separate set of measurements. Since Ω represents a small difference, the necessity for accurate measurements of the periods should be clear. Furthermore, if the system is not exactly at resonance, then an additional constant error equal to (2δ) will be added to the resultant values of Ω, as follows from (47,29c).

The results of the four sets of measurements are shown in Fig. 7, which also displays the theoretical results as described above. Each circled point indicates the average value of the set of ten measurements, while the error bar shows the rms deviation from the average. The agreement

between experiment and theory is quite good, considering the limited extent of these measurements. Since the deviations all lie in one direction, they may indicate a systematic overestimation of $|x_o|$. On the other hand, these deviations could be accounted for if the actual coupling constant λ (as it appears in V_1 of (7b)) were about 5% lower than the theoretical value: $\lambda=3/4$. Since the percentage deviation appears to increase with $|x_o|$, some of the error may be attributed to the neglect of quintic terms in the perturbation.

IX. CONCLUDING REMARKS

An appropriate mathematical technique for analyzing the $\omega_x=2\omega_y$ nonlinear resonance was developed as early as 1913.[9] The coupling action of the resonant elastic pendulum was first discussed in 1933 by Gorelik and Witt, who incompletely analyzed this motion in terms of an "autoparametric" resonance.[10] More recently, the resonant elastic pendulum (along with similar mechanical devices) has been further analyzed by several investigators using a variety of techniques.[11] The analysis used in this paper, however, is based solely on the methods developed previously for treating similar problems in accelerator theory.[2,6] Moreover, our presentation contains several new elements and provides a more comprehensive treatment than found in the earlier work.

Finally, it should be emphasized that this material was specifically designed for inclusion in a modern mechanics course within the physics curriculum.

I am indebted to Dr. Werner Joho of the Swiss Institute for Nuclear Research who introduced the resonant elastic pendulum during his visit here in 1966, and who presented me with the model used in this investigation. I am also indebted to Prof. E. Mettler of Karlsruhe University who, together with Joho, provided the references to the previous investigations cited above.

In conclusion, I wish to acknowledge the invaluable assistance of David A. Johnson who very effectively carried out the computer programming and calculations, as well as the experimental measurements described above.

Table I: Properties of Stable Periodic Modes
(all numbers are multiplied by 100)

x_o	a_2	b_1	a_o	b_3	Ω	E
1.0	1.016	2.934	-0.016	0.006	0.777	0.016
-1.0	-0.986	2.736	-0.014	-0.005	-0.727	0.014
2.0	2.069	6.109	-0.069	0.024	1.622	0.070
-2.0	-1.946	5.316	-0.054	-0.020	-1.417	0.053
3.0	3.169	9.598	-0.168	0.057	2.560	0.173
-3.0	-2.884	7.764	-0.117	-0.043	-2.078	0.113
4.0	4.332	13.512	-0.330	0.111	3.630	0.342
-4.0	-3.802	10.101	-0.199	-0.073	-2.717	0.191
5.0	5.589	18.037	-0.582	0.193	4.902	0.610
-5.0	-4.702	12.342	-0.301	-0.112	-3.340	0.285

REFERENCES

1. See, for example, N. M. Krylov and N. N. Bogoliubov, Introduction to Nonlinear Mechanics, (Princeton Univ. Press, Princeton, 1943).
2. See, for example, A. A. Kolomensky and A. N. Lebedev, Theory of Cyclic Accelerators, (John Wiley & Sons, Inc., New York, 1966), Chap. 3.
3. N. Minorsky, Introduction to Nonlinear Mechanics, (J. W. Edwards, Ann Arbor, 1947), p. 374.
4. A. E. Siegman, Amer. J. Phys. 37, 843 (1969).
5. G. Parzen, Bull. Am. Phys. Soc. 2, 11 (1957).
6. R. Hagedorn and A. Schoch, CERN Report Nos. 57-1, 57-14, (CERN, Geneva, 1957). This work is summarized in Ref. 2.
7. H. Goldstein, Classical Mechanics, (Addison-Wesley Publ. Co., Reading, 1950), Chap. 8.
8. M. M. Gordon, Nucl. Instr. & Meth. 18-19, 281 (1962).
9. H. J. E. Beth, Phil. Mag. 26, 268 (1913).
10. G. Gorelik and A. Witt, Jour. Tech. Phys. USSR 3, 294 (1933); see Ref. 3.
11. E. Mettler, Ingen. Arch. 28, 213 (1959); J. H. Heinbockel and R. A. Struble, Z. Angw. Math. Phys. 14, 262 (1963); P. R. Sethna, J. Appl. Mech. 32, 576 (1965); A. Van der Burgh, J. Mec. (Paris) 7, 507 (1968); T. R. Kane and M. E. Kahn, J. Appl. Mech. 35, 547 (1968).

FIGURE CAPTIONS

Fig. 1: The resonant elastic pendulum discussed in this paper. The scale at left is in cm.

Fig. 2: Trajectory of the pendulum bob during one half of a transfer cycle, as plotted by the computer. This plot is described in Sec. II.

Fig. 3: Set of invariant curves: $K(A,\phi)$ = constant, obtained when system is exactly at resonance ($\varepsilon=0$). The plotted variables are: $v=(A/C)\sin\phi$ vs. $u=(A/C)\cos\phi$.

Fig. 4: Two sets of invariant curves obtained when the off-resonance parameter is given by: $\varepsilon=0.5$ and $\varepsilon=1.0$. Compare with Fig. 3.

Fig. 5: Computed phase space plots obtained for: $C=0.05$, $\varepsilon=0$. The (x,p_x) points are plotted only at those instants when $y=0$, $p_y>0$. These curves should be compared with the theoretical curves of Fig. 3.

Fig. 6: Pairs of nose-up and nose-down parabolic trajectories executed by the pendulum bob when in the stable periodic modes having the energy values: $E=1$, 2, and 5×10^{-3}.

Fig. 7: The fractional frequency change Ω for the stable periodic modes as a function of the initial vertical displacement x_o. The solid curve is obtained from computer results; the straight line is derived from the theory neglecting higher order terms; the circled points with error bars correspond to the experimental measurements.

JP-1

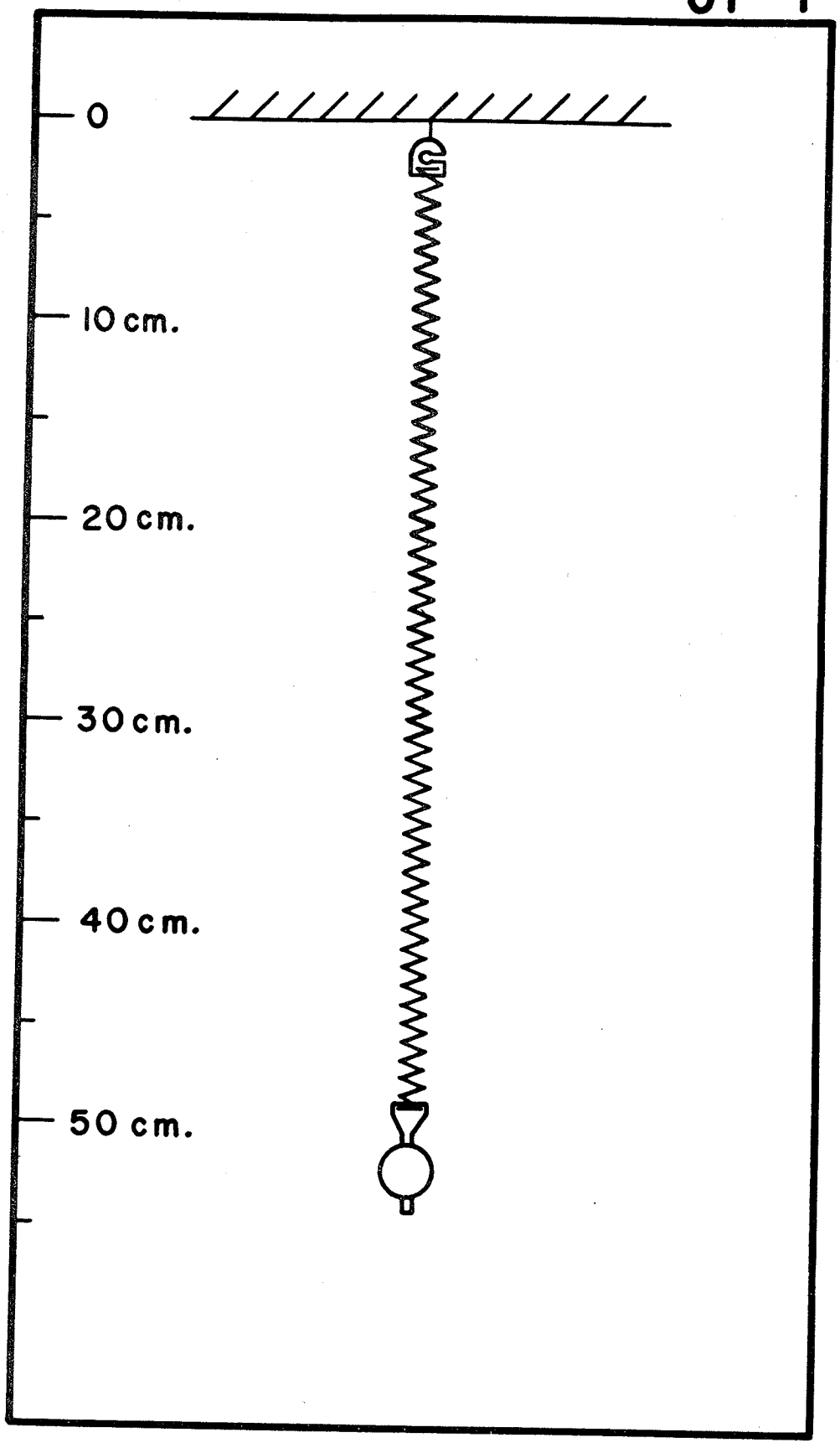

JP-2

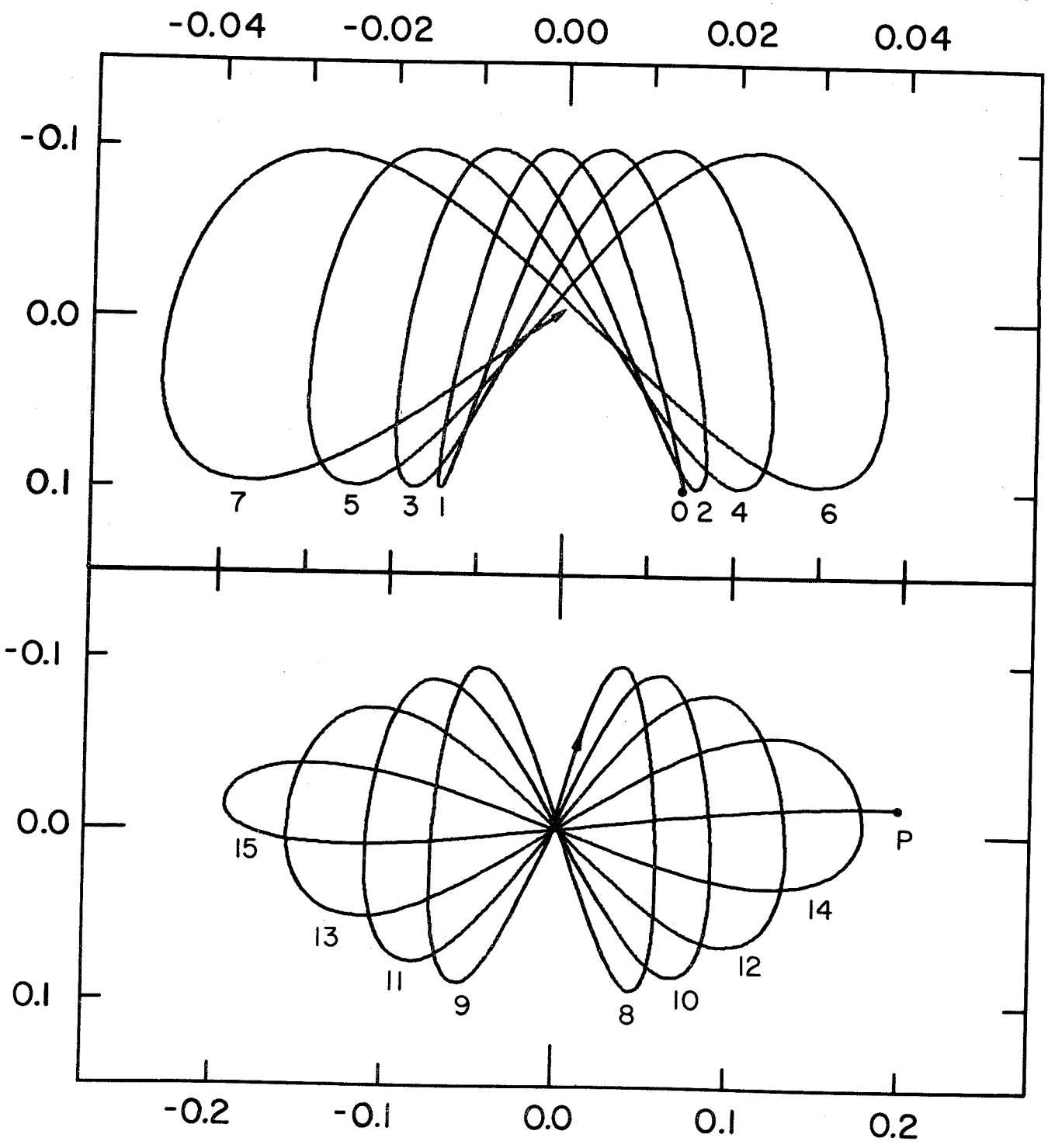
-0.04
-0.02
0.00
0.02
0.04
-0.1
0.0
0.1
7
5
3
1
0
2
4
6
-0.1
0.0
0.1
15
13
11
9
8
10
12
14
P
-0.2
-0.1
0.0
0.1
0.2

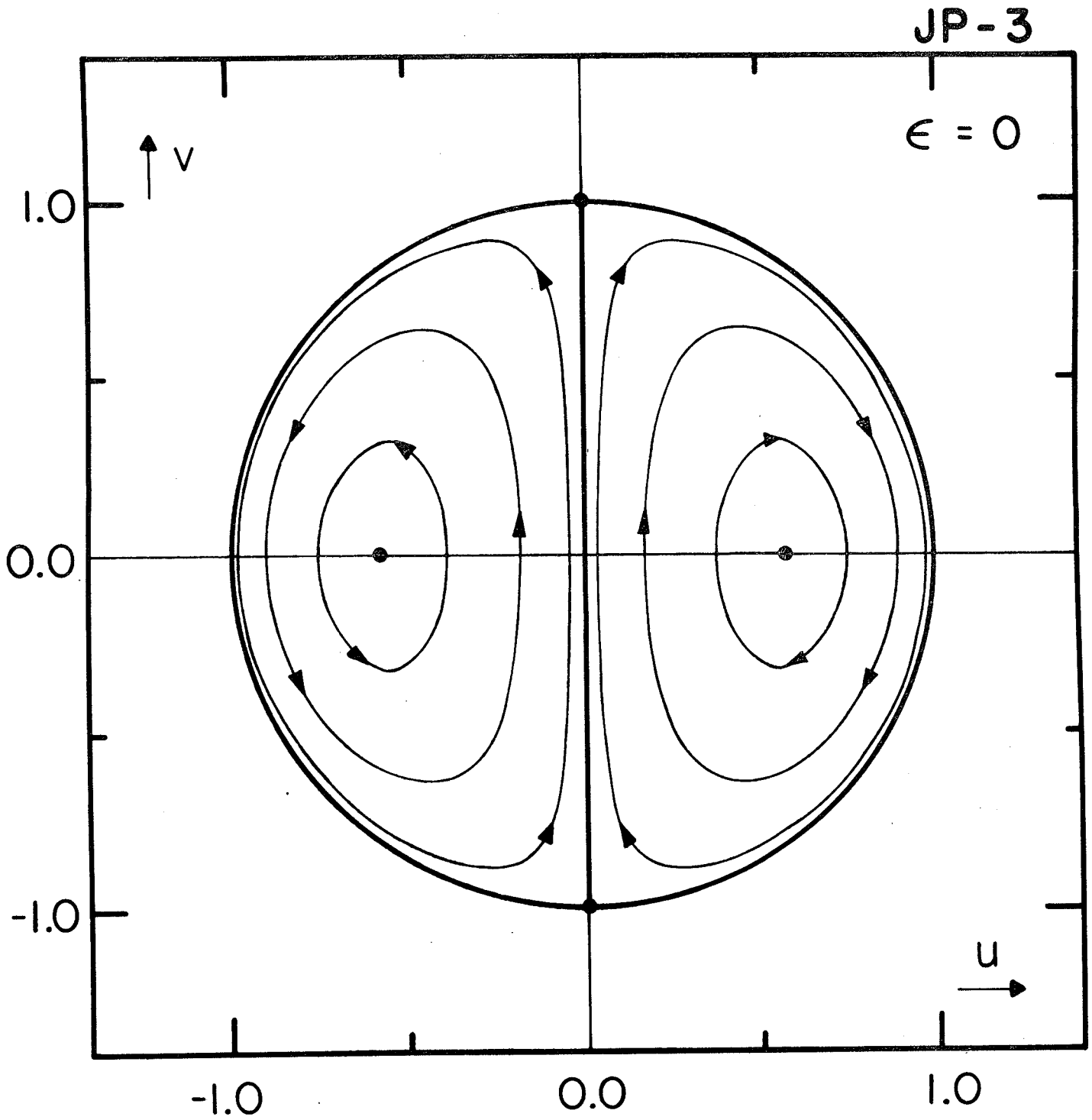
JP-3
ϵ = 0
v
u
1.0
0.0
-1.0
-1.0
0.0
1.0

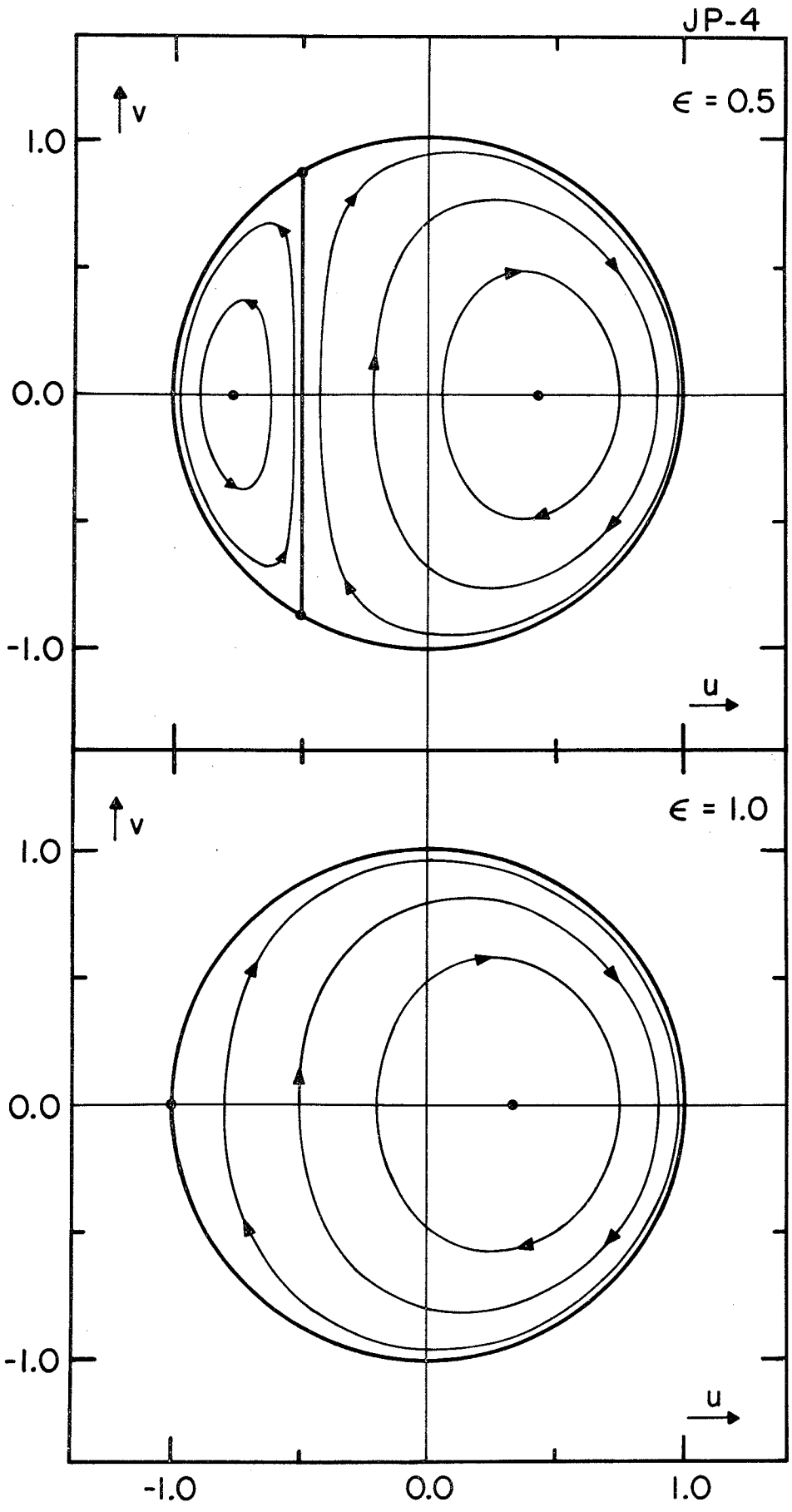
JP-4
ϵ = 0.5
v
u
1.0
0.0
-1.0
ϵ = 1.0
v
u
1.0
0.0
-1.0
-1.0
0.0
1.0

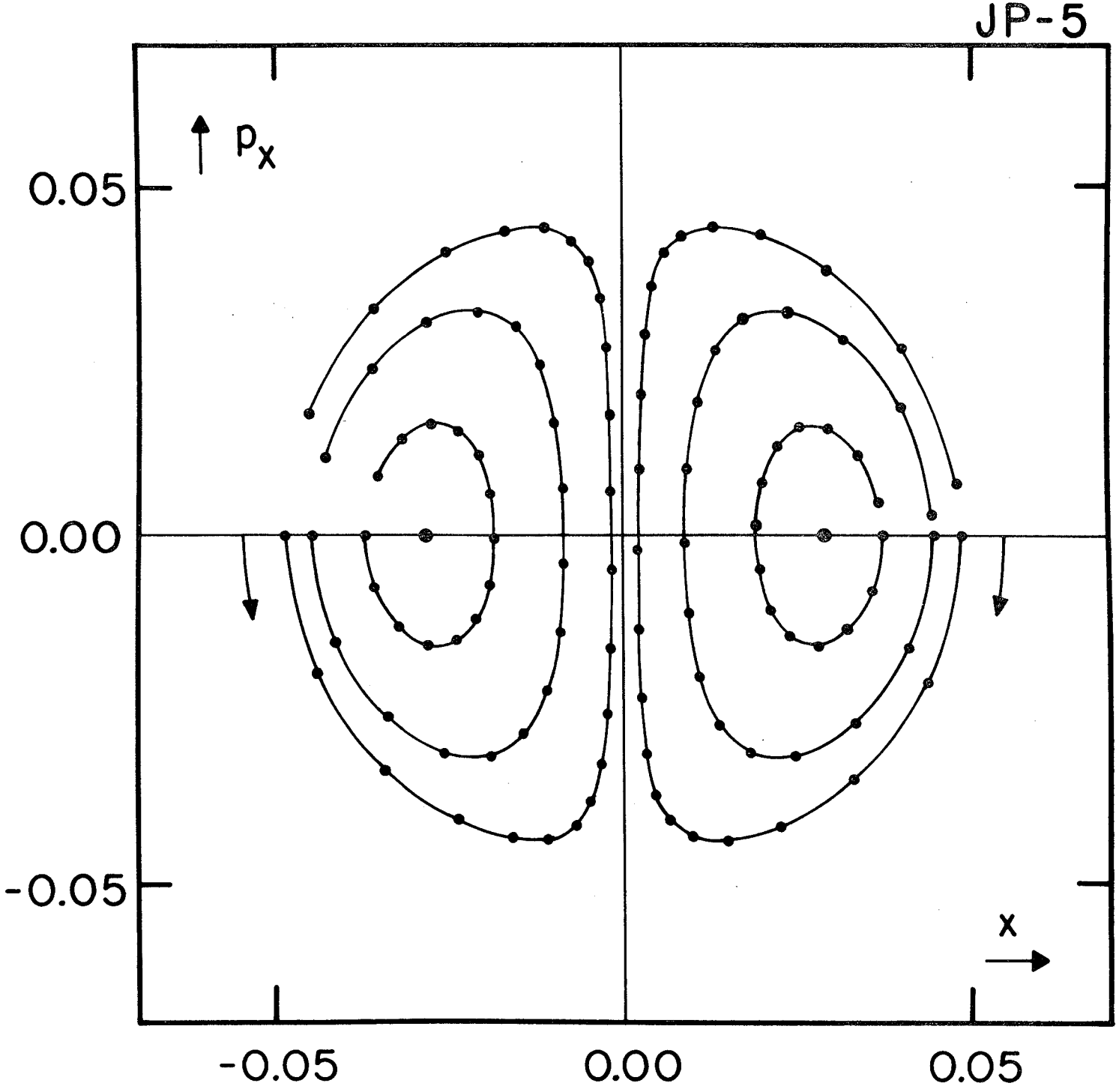
JP-5
p_x
0.05
0.00
-0.05
x
-0.05
0.00
0.05

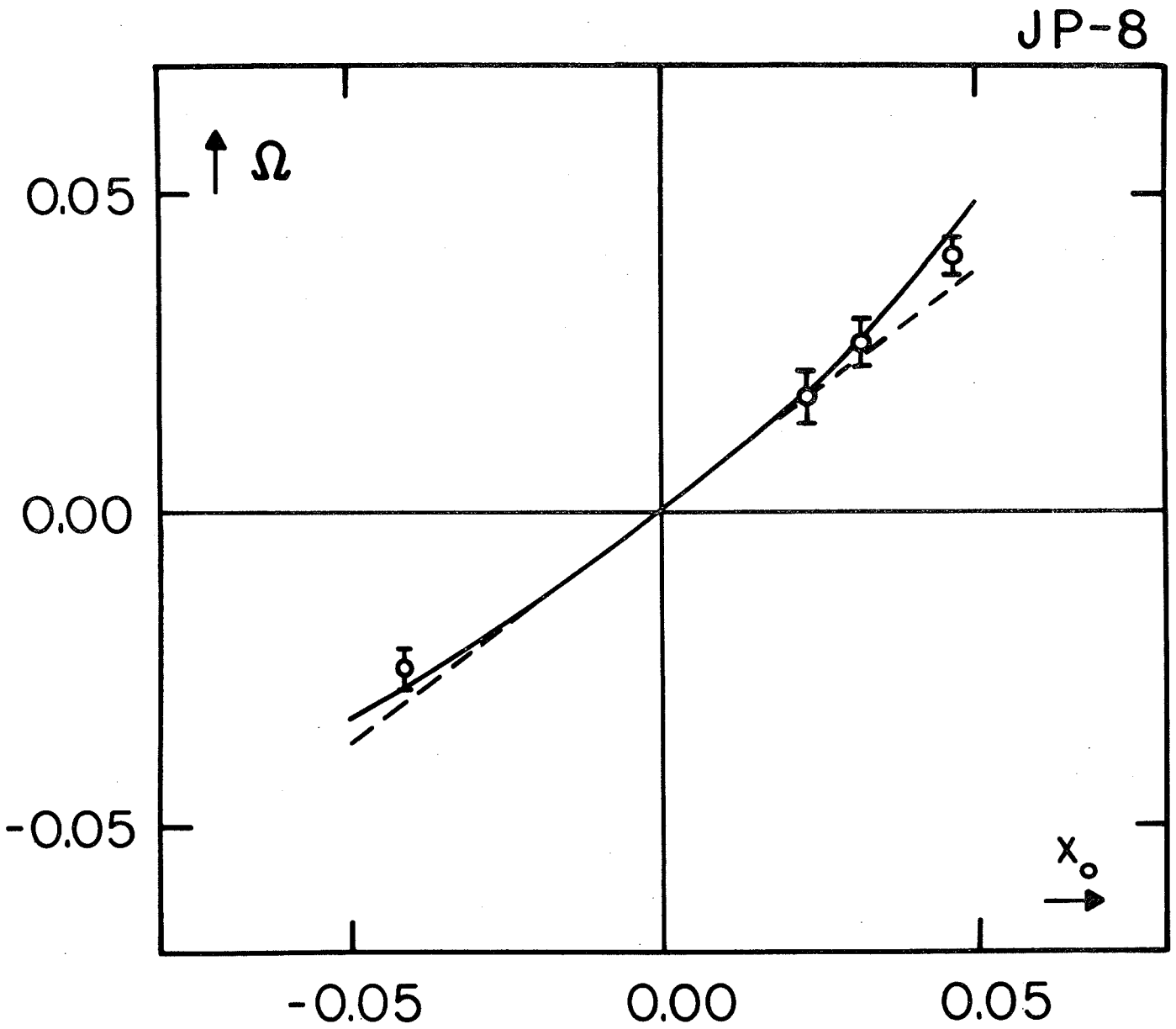
JP-8
Ω
0.05
0.00
-0.05
x_o
-0.05
0.00
0.05